Facultad de Ciencias
Universidad de La Laguna

INSTITUTO ESPAÑOL DE OCEANOGRAFÍA

Diagnosing mesoscale vertical motion and its application in an oceanic cyclonic eddy at the Canary Islands

By Sergio Sicilia González

2022/2023
Final degree project for the major in physics

Supervised by:
Dr. Eugenio Fraile Nuez, Spanish Institute of Oceanography (IEO-CSIC)
Dr. Francisco Javier Expósito González (University of La Laguna, ULL)

CSIC
Consejo Superior de Investigaciones Científicas

GOBIERNO DE ESPAÑA
MINISTERIO DE CIENCIA E INNOVACIÓN

Resumen

Este trabajo de fin de grado constituye una introducción al estudio del campo vertical de velocidades sobre remolinos mesoescalares, estructuras oceanográficas con gran potencial de estudio en el campo de la oceanografía física. Estos remolinos son vitales para entender el comportamiento a gran escala del océano, y realizan importantes tareas como las de transportar nutrientes y diversas sustancias en la columna de agua, o la de distribuir el calor de las capas superficiales a las profundidades del océano. Dentro de estas funciones, los investigadores prestan especial atención a la velocidad vertical, que presenta múltiples retos para su medición por diversos motivos experimentales y por su propia naturaleza débil. El objetivo de este innovador trabajo es el de obtener la velocidad vertical en un remolino ciclónico situado al sur del Hierro. Para ello hemos empleado métodos indirectos como es la denominada ecuación omega, usando datos del modelo IBI de Copernicus, y su validación mediante datos in situ de CTD (conductividad-temperatura-profundidad) tomados en la campaña oceanográfica *Vulcana-III-0222* del Instituto Español de Oceanografía (IEO-CSIC). Los resultados de este trabajo dan cuenta de la posible limitación del modelo IBI, comúnmente usado para estudios oceanográficos, en la obtención de la velocidad vertical en estructuras mesoescalares. Por otro lado el trabajo valida las múltiples utilidades de este modelo, especialmente en los procesos hidrodinámicos horizontales. Este trabajo presenta además, múltiples opciones para futuros trabajos de investigación que podrían sin duda, arrojar más luz sobre diferentes campos y aspectos de la oceanografía física y estudios mesoescalares, aún sin estudiar.

Abstract

This undergraduate thesis constitutes an introduction to the study of the vertical velocity field over mesoscale eddies, oceanographic structures with great potential for study in the field of physical oceanography. These eddies are vital for understanding the large-scale behavior of the ocean, and perform important tasks such as transporting nutrients and various substances in the water column, or distributing heat from the surface layers to the deep ocean. Within these functions, the researchers pay special attention to the vertical velocity, which presents multiple challenges for measurement for various experimental reasons and because of its own weak nature. The objective of this innovative work is to obtain the vertical velocity in a cyclonic eddy located south of El Hierro island. For this we have used indirect methods such as the so-called omega equation, using data from the Copernicus IBI model, and its validation by in situ CTD (conductivity-temperature-depth) data taken in the *Vulcana-III-0222* oceanographic campaign of the Spanish Institute of Oceanography (IEO-CSIC). The results of this work show the possible limitation of the IBI model, commonly used for oceanographic studies, in obtaining the vertical velocity in mesoscale structures. On the other hand, the work validates the multiple utilities of this model, especially in horizontal hydrodynamic processes. This work also presents multiple options for future research that could undoubtedly shed more light on different fields and aspects of physical oceanography and mesoscale studies that have yet to be studied.

Table of Contents

Chapter 1

Motivation and introduction

Resumen:

La circulación oceánica está influenciada por características mesoscalares tales como vórtices, frentes, corrientes en chorro, meandros, anillos, filamentos y remolinos, y comprender su variabilidad es fundamental para su entendimiento. Los remolinos son corrientes de agua que tienen implicaciones significativas en la distribución y transporte de sustancias, y la velocidad vertical desempeña un papel fundamental en estos procesos y en otros, como el transporte de nutrientes, redistribución de biomasa, eliminación de calor de las capas superficiales a las profundidades y la acumulación de microplásticos. Comprender el comportamiento del campo de velocidad vertical es esencial para entender los procesos físico-químicos y biológicos interconectados en el océano. La medición de las velocidades verticales en el océano es un desafío debido a que la magnitud de estas es mucho menor que la de las corrientes horizontales. Para superar esta limitación se han desarrollado métodos indirectos, como la ecuación omega, empleada para inferir la velocidad vertical a partir del campo de velocidad horizontal y densidad. La ecuación omega cuasi-geostrófica y semi-geostrófica son dos versiones de la ecuación que se han utilizado para inferir la velocidad vertical en estructuras mesoescalares con baja ageostrofía, a partir del campo de densidad. Mientras que la ecuación omega generalizada se puede usar independientemente de las condiciones geostróficas del fluido, se requiere de la evaluación simultánea del campo de velocidad y densidad. Un proceso estrechamente relacionado con la formación de estos remolinos es el bombeo de Ekman, que implica mecanismos lineales, no lineales y secundarios. Otro factor relevante es la mezcla vertical, que puede afectar a la velocidad vertical. La comprensión de estos factores es crucial para una mejor comprensión de los procesos oceánicos y sus impactos globales.

1.1 Motivation

Ocean circulation is dominated by a multitude of mesoscale features, such as vortices, fronts, jets, meanders, rings, filaments, and eddies which very frequently observed. Understanding the mesoscale variability is an important key for comprehending ocean circulation (Pascual et al. 2006). Vertical velocity plays a fundamental role in these processes within the mesoscale structures, particularly eddies. Eddies are swirling

currents of water that can form due to various mechanisms (McWilliams 2008), and have significant implications for the distribution and transport of heat, salt, nutrients, and other substances (McGillicuddy 2016). Vertical motion provides essential insights into the dynamics and structure of an eddy, revealing the vertical speed of fluid movement and facilitating the identification of underlying driving processes. Furthermore, vertical fields in mesoscale structures are critical for other various reasons:

1. Vertical velocities in eddies have been observed as a clear factor why nutrients are transported in the euphotic layer (Klein and Lapeyre 2009; Mahadevan 2016), thus changing the structure of plankton communities, and therefore having a major impact on the marine carbon cycle.

2. Vertical velocities in eddies have been responsible of removing heat from the surface to the deep ocean layers. In that sense, authors justify the necessity of examining these vertical movement directly related with processes of heat transport (Gregory 2000).

3. Mesoscale variability redistributes the biomass of zooplankton and mesopelagic fish. In this sense, vertical velocity affects the distribution of biomass in structures such as eddies, tending to distribute in certain areas, which is important for understanding the physical and biological processes that are necessary for good ecosystem management and conservation (Samuelsen et al. 2012).

4. Vertical velocities in eddies are responsible of microplastic transport into the water column. Due to the adherence of a biofilm on the microplastics (biofouling), a sinking process is produced, which depends on the physical characteristics of these particles and the conditions of the vertical velocity field. Microplastics experience sinking or oscillation on eddies, leading to a concentration peak at intermediate depths based on size, impacting ecosystems (Kooi et al. 2017).

Undoubtedly, giving greater consideration to the behavior of the vertical velocity field of a fluid is a crucial aspect of physical oceanography. This approach not only helps us to gain a better understanding of the physical processes taking place in the ocean but also sheds light on the interconnections between other physical-chemical and biological processes.

1.2 Introduction

Measuring vertical velocities in the ocean is a challenging task because the magnitude of the vertical velocity is much smaller than that of the horizontal velocity, with $\omega \sim 10\ m\ day^{-1}$ for mesoscale and $\omega \sim 100\ m\ day^{-1}$ for submesoscale (Mahadevan and Tandon 2006). Measurements of vertical velocity in the ocean have been carried out using tracer release experiments and Lagrangian measurements of isopyclic drifts (Hansen et al. 1987; S. S. Lindstrom and D. P. Watts 1994; Harcourt et al. 2002). Although

these methods provide estimates of the vertical velocity, they lack detailed information on the fields and constituent forces. To overcome this issue, indirect methods, such as the omega equation, have been developed to infer the vertical velocity from the horizontal velocity and density field (Viúdez et al. 1996).

Methods for inferring vertical velocity in geophysical fluids were first implemented in the atmosphere, where quasi-geostrophic theory (QG) was applied using a Q vector for models with small Rossby numbers (Hoskins et al. 1978). In this theoretical framework, ageostrophic motion tends to restore the thermal wind balance that geostrophic motion tends to disturb, leading to the vertical velocity. Subsequently, the QG omega equation was applied in the study of mesoscale eddies in the Alborán Sea, as it only requires the density field and related variables (Joaquín Tintoré et al. 1991). Despite the potential of this method, there have been very few studies that inferred vertical velocity in mesoscale structures, and even fewer in the Atlantic, such as Pascual et al. (2015); Benítez-Barrios et al. (2011a) and Barceló-Llull et al. (2016).

The objective of improving the accuracy of the omega equation let to the development of a more comprehensive version that accounts for ageostrophic advection. This modified equation is known as the semi-geostrophic (SG) omega equation (Brian J. Hoskins and Ion Draghici 1977). Similar to the quasi-geostrophic (QG) form, the SG equation also relies on information about the density field. However, it addresses a limitation of the QG approach, with can introduce systematic biases when horizontal stability and potential vorticity vary significantly. This problem can arise when the Rossby number becomes larger, invalidating the quasi-geostrophic theory (Pinot et al. 1996; Pedder and Thorpe 1999). Overall, the SG omega equation offers an improved method for obtaining accurate estimates of vertical velocity in geophysical fluids, particularly in cases where the QG approach may not be adequate.

Before the introduction of the Q vector by Hoskins et. al (1978) in the QG omega equation, it suffered from a cancellation of forcing terms that hindered the determination of relative forces (Trenberth 1977). This issue arose because the local, rather than material, derivatives of the geostrophic differential vorticity were matched. To address this problem, a new formulation was proposed in terms of the rate of change of differential relative vorticity in a fluid parcel, resulting in the generalized omega equation (hereafter generalized). This equation highlights the role of differential ageostrophic vorticity change and differential divergence in driving nonquasigeostrophic vertical velocity and vorticity, respectively (Viúdez et al. 1996). Numerical experiments have since demonstrated that the generalized form yields more accurate estimates of vertical velocity (Viúdez and Dritschel 2004).

This version of the omega equation offers numerous advantages over the QG and SG forms as it is less restrictive can determine vertical velocity in high ageostrophic environments. However, there is a caveat, the horizontal velocity and density field must be evaluated simultaneously. This can pose a challenge when trying to infer vertical velocity in the ocean from in situ data, as obtaining these fields would require multiple devices. For instance, the Shipboard Acoustic Doppler Current Profiler (SADCP) could be

used to obtain the horizontal velocity, which would need to be used in conjunction with a Conductivity-Temperature-Depth (CTD) sensors along a regular grid of hydrographic stations, or with the use of a vessel tow-Seasoar with coupled CTD to obtain the density field.

The diagnosis of vertical velocity in mesoscale frontal regions is only possible through vertical cross-sections of density and horizontal velocity for the QG and SG (generalized) form, given that the flow is linear along the front. Two- and three-dimensional diagnostics have contributed to a better understanding of the ageostrophic secondary circulation (ASC), which includes ageostrophic horizontal and vertical velocity, and related processes in these regions (Pallàs-Sanz et al. 2010a,b). However, eddies have a nonlinear flow, requiring a three-dimensional quasi-synoptic grid of the aforementioned fields to obtain the generalized omega equation. The properties of mesoscale eddies vary globally, with sizes ranging from 20 to 300 km, making it difficult to sample them and resulting in limited ASC studies in eddies (Klocker and Abernathey 2014). For examples, Allen and Smeed (1996) solved the QG omega equation, using SeaSoar sampled data, to obtain the vertical velocity at the Iceland-Færœs front, which exhibed a dipole pattern in the vertical velocity structure. Similarly, Benítez-Barrios et al. (2011b) estimated the QG vertical velocity in an intrathermocline eddy, a swirling current created by mixing hot and cold water, in the northwest of the African coastal transition zone, revealing a dipolar pattern in their low-resolution data with a downward (upward) zone on the western (eastern) side. Nardelli (2013) estimated the vertical velocity of an eddy using the SG omega equation, with satellite-in-situ reconstructed data, and found that the vertical velocity field had a dipole pattern within the eddy core and an octopolar pattern along the eddy periphery, consisting of alternating upward and downward cells.

When examining ASC in mesoscale eddies, much of the research is focused on self-induced Ekman pumping, a process closely tied to the formation of these mesoscale eddies. Three observed mechanisms are associated with this process (Gaube et al. 2015). The first is linear Ekman pumping, which results from the difference in velocity between the ocean and surface winds and the resulting wind stress curl. This generates Ekman upwelling in icyclonic centers and Ekman downwelling in anticyclonic centers (Gaube et al. 2015; Martin and Richards 2001). The second mechanism, known as nonlinear Ekman pumping, occurs when surface wind stress with the surface geostrophic vertical vorticity gradient, resulting in mesoscale Ekman upwelling and downwelling dipoles (Stern 1965; Gaube et al. 2015). The third mechanism is secondary and arises from the eddy-induced sea surface temperature (SST) gradient, which generates stress curvature and therefore Ekman pumping in regions with gradients transverse to the wind (Chelton and Xie 2010; Gaube et al. 2015).

One important factor that affect the vertical velocity is vertical mixing, which involves the movement of water from different depth towards the surface or the bottom. In an eddy, rotational and divergent flow patterns can alter the vertical mixing, making it a crucial factor to consider. However, not many studies have focused on the effects of mixing on vertical motions, partly due to noise propagation through higher-order derivatives, nonlinear effects, and the significant dependence on mixing parameters in the general formulation (Estrada-Allis et al. 2019). Nagai et al. (2006) demostrated that

vertical mixing significantly increases ASC in the first 100 meters of the ocean, which is non-negligible for certain values. Furthermore, Pallàs-Sanz et al. (2010b), using a generalized diabatic omega equation, confirmed that the vertical mixing also increases the vertical velocity in the first 100 meters of the ocean.

To sum up, measuring vertical velocities in the ocean can be challenging, but researchers have developed indirect methods, such as the QG and SG (generalized) omega equation, to infer vertical velocity from the horizontal velocity and density field. These methods have been successfully applied to investigate mesoscale eddies and fronts, which exhibit varying properties worldwide. The aim of this undergraduate thesis is to assess the vertical velocity of a mesoscale eddy using the generalized omega equation, while considering ASC, Ekman pumping, and vertical mixing processes.

Chapter 2

Data and methods

Resumen:

En este capítulo se explican los datos que se han utilizado, así como los desarrollos teóricos y metodológicos del trabajo. Se usaron datos de CTD (conductividad-temperatura-profundidad) en el interior de un remolino ciclónico adquiridos durante la campaña oceanográfica *Vulcana-III-0222* del Instituto Español de Oceanografía (IEO-CSIC) en febrero de 2022 al sur de El Hierro. Además, se usaron datos del modelo de Copernicus IBI para la fecha en la que se realizó el muestreo in situ. Estos datos proporcionan información del campo de velocidad de la corriente, temperatura y salinidad, con una alta resolución horizontal, pero una resolución vertical heterogénea. Para intentar solventar estos problemas metodológicos iniciales, se realizaron interpolaciones cúbicas a los datos de IBI para obtener una malla tridimensional regular comparable con los datos in situ. Se derivó además la ecuación omega generalizada para fluidos no viscosos, isoentrópicos y de Boussinesq, a partir de las ecuaciones de vorticidad. Para resolver esta ecuación en derivadas parciales se aplicó el método numérico de las diferencias finitas para unas condiciones óptimas de frontera. Todo el cálculo numérico, así como las representaciones gráficas, se llevaron a cabo en Matlab y haciendo uso de la librería EOS-80 para los cálculos de termodinámica.

The objective of this work is solving the vertical velocity field of a cyclonic eddy with the use of CTD (conductivity-Temperature-Depth) profilers. These data were obtained in February 2022 south of the island of El Hierro during the realization of *Vulcana-III-0222* oceanographic cruise from the Spanish Institute of Oceanography (IEO-CSIC) and on board R/V Ángeles Alvariño. The eddy was detected via satellite in October 2021 using sea level anomaly (SLA) data. Its formation started as a filament in northwest Africa and evolved for 5 months until it reached the southeast of the island of El Hierro, where it was finally sampled on February 16, 2022.

2.1 Hydrography

Conductivity, Temperature and Pressure data were obtained in the first 1200 m depth of the water column with a CTD *SeaBird 911-plus*. The CTD was equipped with a dual temperature and conductivity sensors, with accuracies of $0.001\ ºC$ and $0.0003\ S/m$, respectively. Other sensors were added to the CTD as: dissolved oxygen, pH, ORP, turbidity, and fluorescence. All sensors were calibrated before and after the cruise. Six CTD stations were carried out during the oceanographic cruise Vulcana-III-0222 (Figure 1). Regarding the horizontal speed, it was not measured due to the SADCP being damaged.

2.2 Velocity and density field model

The daily horizontal velocity, temperature and salinity field numerical outputs for the dates when the in situ CTD stations were performed were performed were taken from Marine Copernicus Atlantic Ocean Analysis and Forecasting - Iberian Biscay Irish (IBI) (https://marine.copernicus.eu). Nologin runs the model daily in collaboration with Puertos del Estado and the Galician Supercomputing Center (CESGA) provides the computing resources. The dataset gives a 5-day hydrodynamic forecast that includes significant high frequency processes that are essential for characterizing marine operations in the region (e.g., tidal forces, swells, and high-frequency atmospheric forces, river runoff). Furthermore, a weekly update of the truncated IBI analysis is available as an upgraded historical IBI appraisal (Sotillo et al. 2015). The system is based on the eddy-resolving NEMO model operating at a horizontal resolution of 1/36° (≈2-3 km) (Pierre et al. 2008). The data is distributed vertically in 50 z-levels with a resolution ranging from roughly 1 m in the top 10 m to more than 400 m in the deep ocean.

As for the treatment of the IBI data, cubic interpolations in longitude and latitude were carried out to increase the horizontal resolution of the data to 1 km. The depth data was also interpolated to have a regular grid with a resolution comparable to that obtained with CTD stations (~5 m).

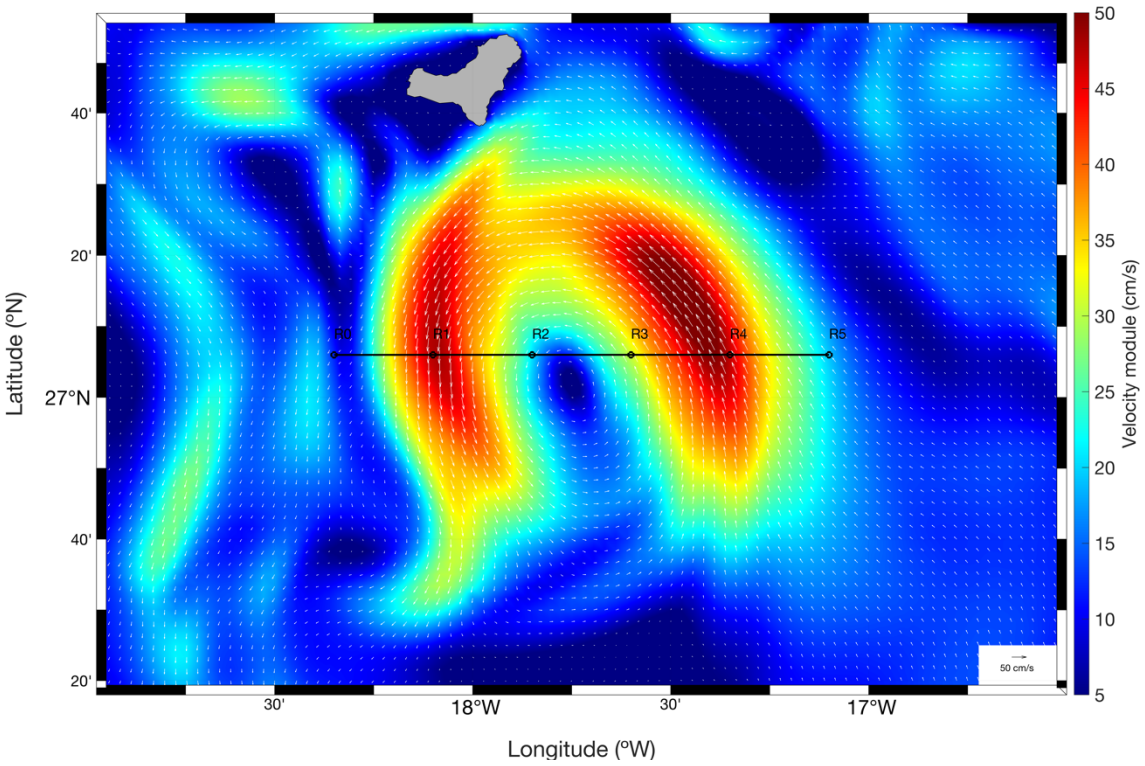

Figure 1: State of the eddy on February 16, 2022. The white vectors are the horizontal current velocity of the first depth level of the IBI data, the colormap represents the velocity module of this current, the black line is the path followed by the oceanographic vessel and the black dots are the CTD sampling stations with its label.

2.3 The generalized ω equation

A brief derivation of the generalized omega equation for non-viscous, isentropic, and Boussinesq fluids is presented. The detailed formulation can be found in Viúdez et al. 1996.

As it has been previously discussed, the omega equation is the equation for the rate of change of the differential ageostrophic vorticity. Therefore, by calculating the ratio of change of total differential vorticity and geostrophic vorticity the omega equation can be obtained as the difference of both terms, $\zeta_z^a = \zeta_z - \zeta_z^g$ (where the subscript indicates hereinafter the partial derivative with respect to z).

The geostrophic and ageostrophic horizontal velocities, respectively, are given as:

$$\boldsymbol{u}_h^g = -\alpha_0 f^{-1} \boldsymbol{k} \times \boldsymbol{\nabla_h} \emptyset \quad (1)$$

$$\boldsymbol{u}_h^a = \boldsymbol{u}_h - \boldsymbol{u}_h^g \quad (1)$$

where $\alpha_0 = 1/\rho_0$, being ρ_0 the reference density at atmospheric pressure, $f = 2\Omega \, sin\, \theta_0$ is the Coriolis parameter at the mean latitude θ_0, and Ω the constant value of the earth's rotational velocity, $\boldsymbol{k}$ the vertical unit vector, $\boldsymbol{\nabla}_h \equiv (\partial_x, \partial_y)$ the horizontal gradient, $\emptyset$ the geopotential and $\boldsymbol{u}_h$ the total horizontal velocity. The horizontal momentum, volume conservation, and thermal wind equations are:

$$\frac{d\boldsymbol{u}_h}{dt} + f\boldsymbol{k} \times \boldsymbol{u}_h^a = 0 \tag{3}$$

$$\boldsymbol{\nabla} \cdot \boldsymbol{u} \; = \; 0 \tag{4}$$

$$\frac{d\varrho}{dt} = 0 \tag{5}$$

$$f\boldsymbol{k} \times \boldsymbol{u}_{hz}^g = \boldsymbol{\nabla}_h \varrho \tag{6}$$

where $\boldsymbol{u} \equiv (u, v, \omega)$ is the total Eulerian velocity field, $\varrho = \rho g \alpha_0$ the buoyancy, where ρ is the density of the fluid and g the gravitational acceleration. The rate of change of the total vorticity can be obtained taking the vertical component of the curl of the horizontal momentum equation, $\boldsymbol{k} \cdot \boldsymbol{\nabla}_h \times (3)$, according to the following equation:

$$\frac{d\zeta}{dt} = (f + \zeta)\frac{\partial \omega}{\partial z} + \boldsymbol{\zeta}_{ph} \cdot \boldsymbol{\nabla}_h \omega \tag{7}$$

where $\zeta = \frac{\partial v}{\partial x} - \frac{\partial u}{\partial y}$ and $\boldsymbol{\zeta}_{ph} \equiv \boldsymbol{k} \times \boldsymbol{u}_{hz} = \left(-\frac{\partial v}{\partial z}, \frac{\partial u}{\partial z}\right)$ are the relative vorticity and pseudovorticity equations, respectively. Applying the horizontal gradient to (5) we obtain the rate of change of the horizontal density gradient:

$$\frac{d\boldsymbol{\nabla}_h \varrho}{dt} = -\boldsymbol{\nabla}_h \cdot \boldsymbol{u}_h \boldsymbol{\nabla}_h \varrho - \frac{\partial \varrho}{\partial z}\boldsymbol{\nabla}_h \omega \tag{8}$$

The rate of change of the differential geostrophic vorticity equation, $\zeta_z^g = -f^{-1}\boldsymbol{\nabla}_h^2 \varrho$, can be obtained taking the horizontal divergence of (8):

$$\frac{d\zeta_z^g}{dt} = 2f^{-1}\left[\boldsymbol{\nabla}_h \boldsymbol{u}_h : \boldsymbol{\nabla}_h(\boldsymbol{\nabla}_h \varrho) + \boldsymbol{\nabla}_h \omega \cdot \boldsymbol{\nabla}_h \frac{\partial \varrho}{\partial z}\right] + f^{-1}\boldsymbol{\nabla}\varrho \cdot \boldsymbol{\nabla}_h^2 u \tag{9}$$

where $\boldsymbol{A}$: $\boldsymbol{B}$ is the scalar double-dot of two dyadics. Letting $\boldsymbol{A} = \sum_i \boldsymbol{a}_i \boldsymbol{b}_i$, and $\boldsymbol{B} = \sum_j \boldsymbol{c}_j \boldsymbol{d}_j$, the double dot product is $\boldsymbol{A}: \boldsymbol{B} = \sum_{i,j}(\boldsymbol{a}_i \cdot \boldsymbol{c}_j)(\boldsymbol{b}_i \cdot \boldsymbol{d}_j)$.
The omega equation for the rate of change of the differential ageostrophic vorticity can be obtained from the derivative of (7), and (9):

$$\frac{d\zeta_z^a}{dt} = -f^{-1}\boldsymbol{\nabla}_h \cdot \left[2\boldsymbol{Q}_h + \frac{\partial \varrho}{\partial z}\boldsymbol{\nabla}_h \omega\right] + (f + \zeta)\frac{\partial^2 \omega}{\partial z^2} \tag{10}$$

$$+\boldsymbol{\zeta}_{phz}^a \cdot \boldsymbol{\nabla}_h \omega - \boldsymbol{\zeta}_{ph}^a \cdot \boldsymbol{\nabla}_h^2 u_h$$

where $\boldsymbol{\zeta}_{ph}^{a} \equiv \boldsymbol{k} \times \boldsymbol{u}_{h}^{a} = \left(-\frac{\partial v^{a}}{\partial z}, \frac{\partial u^{a}}{\partial z}\right)$ is the horizontal ageostrophic pseudovorticity. The $\boldsymbol{Q}$ vector, $\boldsymbol{Q}_{h} \equiv \boldsymbol{\nabla}_{h} \cdot \boldsymbol{u}_{h} \boldsymbol{\nabla}_{h} \varrho$, has also been introduced. Therefore, the divergence of this vector is evaluated as:

$$\boldsymbol{\nabla}_{\mathrm{h}} \cdot \mathbf{Q}_{\mathrm{h}} = \boldsymbol{\nabla}_{\mathrm{h}} \mathbf{u}_{\mathrm{h}} \colon \boldsymbol{\nabla}_{\mathrm{h}} (\boldsymbol{\nabla}_{\mathrm{h}} \varrho) + \boldsymbol{\nabla}_{\mathrm{h}} \varrho \cdot \boldsymbol{\nabla}_{\mathrm{h}}^{2} \mathrm{u}_{\mathrm{h}} \tag{11}$$

To solve this partial differential equation (PDE) in terms of the ω variable some approximations must be made in (10). Neglecting the following terms:

(i) The material rate of change of ζ_{z}^{a},
(ii) The terms $\boldsymbol{\zeta}_{phz}^{a} \cdot \boldsymbol{\nabla}_{h} \omega$ and $\boldsymbol{\nabla}_{h} \varrho_{z} \cdot \boldsymbol{\nabla}_{h} \omega$,
(iii) The horizontal changes of ϱ, so that $\varrho_{z} \boldsymbol{\nabla}_{h}^{2} \omega \approx -N^{2} f^{-1} \boldsymbol{\nabla}_{h}^{2} \omega$, where N^{2} is the squared root of the Brunt-Väisälä frequency, $N^{2} = -g \alpha_{0} \frac{\partial \rho}{\partial z}$.
(iv) As $\left|\zeta_{phz}^{a}\right| > \left|\zeta_{phz}^{g} = f^{-1} \nabla_{h} \varrho_{z}\right|$, $\nabla_{h} \varrho_{z} \cdot \nabla_{h} \omega$ can be neglected, leading to the approximation $\nabla_{h} \cdot (\varrho_{z} \nabla_{h} \omega) \approx \varrho_{z} \nabla_{h}^{2} \omega$

The generalized ω equation (10), in terms of the $\boldsymbol{Q}$ vector is simplified to:

$$\mathrm{N}^{2} \nabla_{\mathrm{h}}^{2} \omega + \mathrm{f}(\mathrm{f} + \zeta) \frac{\partial^{2} \omega}{\partial \mathrm{z}^{2}} = 2 \boldsymbol{\nabla}_{\mathrm{h}} \cdot \mathbf{Q}_{\mathrm{h}} + \mathrm{f} \boldsymbol{\zeta}_{\mathrm{ph}}^{\mathrm{a}} \cdot \boldsymbol{\nabla}_{\mathrm{h}}^{2} \mathbf{u}_{\mathrm{h}} \tag{12}$$

which can be solved assuming that both $\boldsymbol{u}_{h}$ and ϱ are known.

2.4 Numerical solution of the $\boldsymbol{\omega}$ equation

As seen in the previous section, the omega equation is an elliptic PDE. Given the success in solving the poison equation in 3 dimensions by relaxation methods (Houtman et al. 1994; Zhang 1998), such as the finite difference method, the omega equation is solved in this way, given suitable boundary conditions (Leach 1987; Pollard and Regier 1992; Allen and Smeed 1996). The conditions at the top and bottom of the grid are: $\omega|_{z=0} = \omega|_{z=700} = 0$; on the sides, conditions of random values close to zero have been provided, so that the numerical solution converges to the internal values of the grid.

As it is usual in numerical methods, the space domain has been split in a 3 dimensional discrete grid , $x_{i,j,k}$. A uniform partition is assumed, in coordinates i, j, since as mentioned in **section 2.2**, the horizontal resolution of the IBI data is constant. However in coordinate k, the resolution varies with the depth value, so a priori it cannot be considered as uniform. Splitting the known parameters of equation (12)

$$A(x_i, y_j, z_k) = N^2 \tag{13}$$

$$B(x_i, y_j, z_k) = f(f + \xi) \tag{14}$$

$$C(x_i, y_j, z_k) = 2\boldsymbol{\nabla}_h \cdot \boldsymbol{Q}_h + f\boldsymbol{\xi}_{ph}^a \cdot \boldsymbol{\nabla}_h^2 \boldsymbol{u}_h \tag{15}$$

The numerical solution of (12) by the finite difference method is:

$$\begin{aligned} &\frac{A(x_i, y_j, z_k)}{h^2} \cdot \Big(F(x_{i+1}, y_j, z_k) + F(x_{i-1}, y_j, z_k) + F(x_i, y_{j+1}, z_k) \\ &\qquad + F(x_i, y_{j-1}, z_k) - 4F(x_i, y_j, z_k)\Big) + \\ &\frac{B(x_i, y_j, z_k)}{\Delta z^2} \cdot \Big(F(x_i, y_j, z_{k+1}) + F(x_i, y_j, z_{k-1}) - 2F(x_i, y_j, z_k)\Big) \\ &\qquad = \mathrm{C}(x_i, y_j, z_k) \end{aligned} \tag{16}$$

where $F(x_i, y_j, z_k)$ is the solution of the (12) omega equation. The h and Δz values are the resolutions of the $x - y$ and z axis respectively.

The numerical calculation of the associated parameters to solve the omega equation, as well as the numerical resolution itself was carried out using *Matlab* (https://es.mathworks.com) calculation tools and the EOS-80 thermodynamic equations of state library for *Matlab* (P. Morgan 1994).

Chapter 3

Results and discussion

Resumen:

En este capítulo se exponen los resultados obtenidos con los datos del modelo IBI, así como una comparación con los datos in situ. Se obtiene que los resultados de los parámetros necesarios para resolver la ecuación en derivadas parciales son coherentes con lo esperado en un remolino ciclónico y que, además, algunos de estos parámetros presentan una estructura que parece indicar que existe un error de fondo. Esto produce que no se pueda determinar claramente un patrón en el resultado de la velocidad vertical, pero que permite vislumbrar cierta información, como su rango de valores. La causa de este patrón se puede atribuir a una suavidad en los valores de salida del modelo IBI, así como a su baja resolución vertical.

3.1 Results

3.1.1 Geostrophic velocity

Figure 2 shows a comparison between the geostrophic velocity obtained from the in situ CTD station data and the temperature, conductivity and pressure data obtained from IBI model and interpolated to the coordinates and depths of the in situ CTD stations, which we shall refer to as the pseudo-stations. As it can be seen in the figure, the IBI data for the pseudo-stations captures the eddy structure in a manner consistent with the CTD stations, although the velocity profiles have a stylized appearance typical of model-derived data. This finding is also consistent with the expected rotational direction of eddies in the northern hemisphere, which is anticlockwise (clockwise) for cyclonic (anticyclonic) eddies.

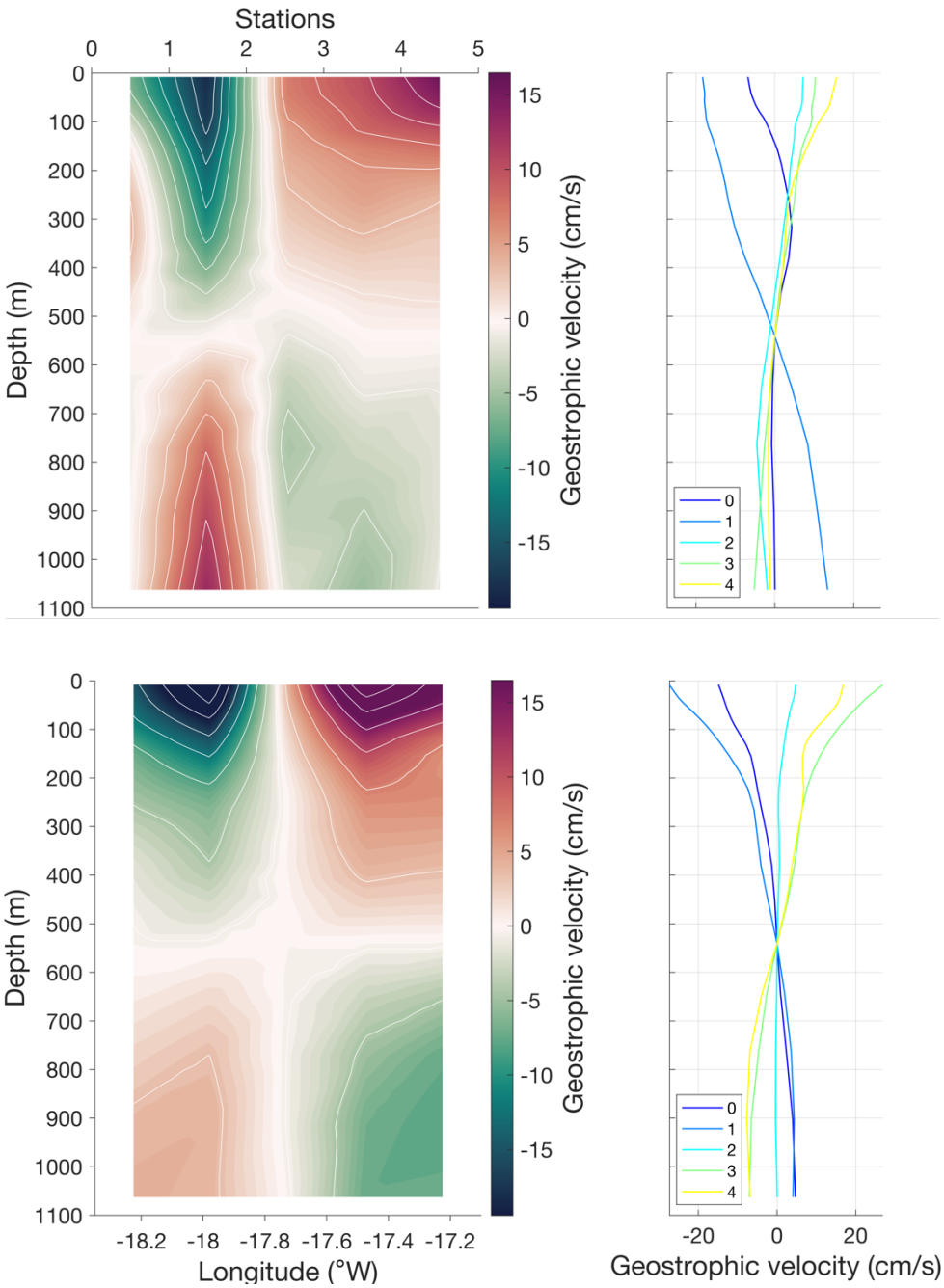

Figure 2: The upper figures are the contour, with the station labels on top, and geostrophic velocity profile from the in situ data, and the lower figures are the pseudo-stations from the IBI data. The white curves in the contours represent a 4 cm/s variation of the geostrophic velocity.

The observed rotation pattern of the eddy is visible to the first 600 meters depth or a isopicnal of 27.3 $kg \cdot m^{-3}$. The resulting eddy has an anticlockwise rotation with geostrophic velocities from -20 to 20 cm/s. However, above this level, others factors as friction, changes of the water mases and/or topography may contribute to change in the rotation pattern and a decrease in the intensity of the geostrophic velocity.

3.1.2 Analysis of the parameters

The first parameter of the generalized omega equation is the Brunt-Väisälä frequency, which is a measure of the vertical stability of the stratified fluid. In the ocean, this can be obtained from variations in density and water temperature. Cyclonic eddies are associated with upwelling, a process that brings colder and nutrient-rich waters to the surface (Ning et al. 2004). As a result, the vertical mixing is altered, leading to an increase in the Brunt-Väisälä frequency in the upper layers of the ocean.

Figure 3 shows a general trend where the frequency increases as the proximity to the surface intensifies. At approximately 50 meters depth, the isopycnal exhibits a significant variation, which coincides with the frequency reaching its maximum.

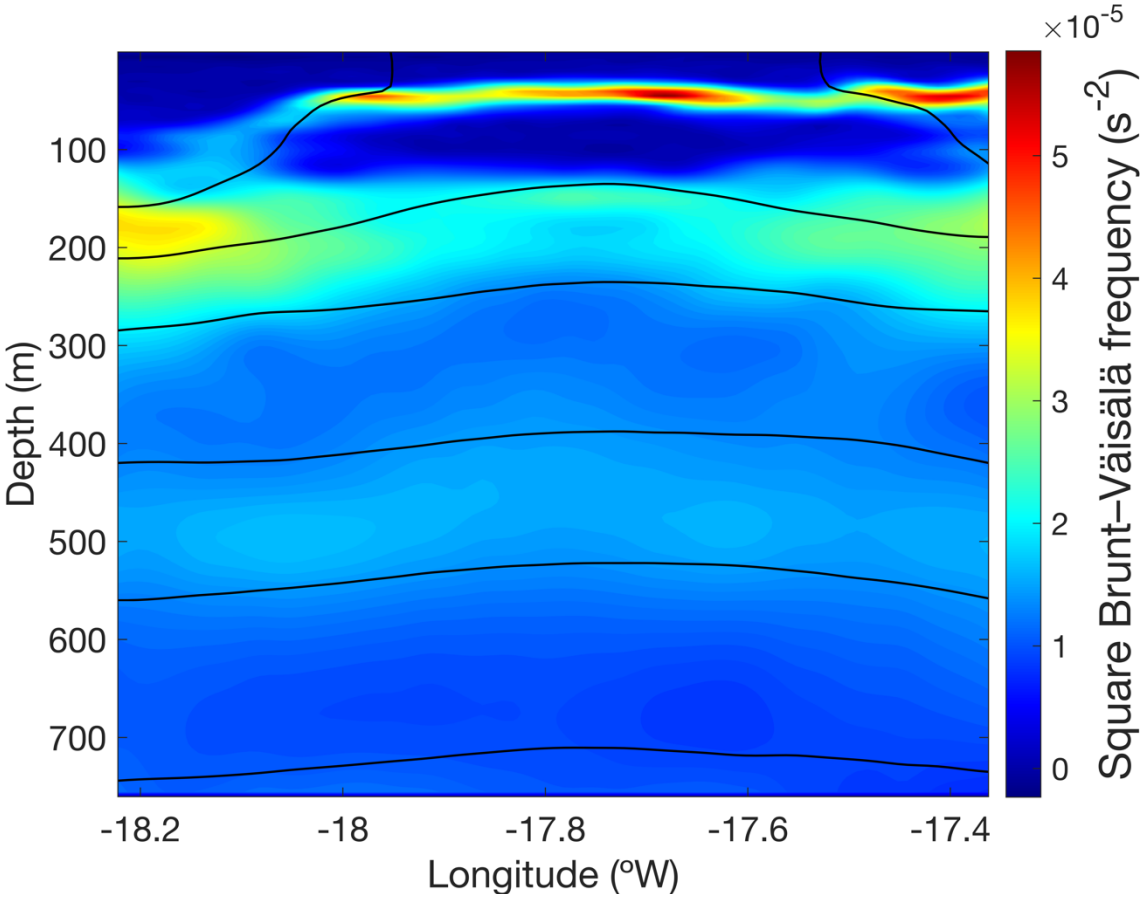

Figure 3: Brunt-Väisäla frequency using IBI data for the eddy water column at a latitude that intersects with the eddy center. The black lines represent isopycnals every 0.2 $kg \cdot m^{-3}$.

The next term is the total vorticity, which is a combination of the vorticity due to the rotation of the earth and the vorticity of the eddy itself. The total vorticity of a cyclonic eddy affects the vertical velocity of the eddy by creating an imbalance between the advection and stretching vorticity forcing terms (Estrada-Allis et al. 2019).

This imbalance is further accentuated in regions where the relative vorticity is locally enhanced and coupled with lateral density variations (Mahadevan et al. 2008).

As shown in Figure 4, the total vorticity is highest at the center of the eddy, at about -17.7°W, and decreases both at depth and at the edges of the eddy.

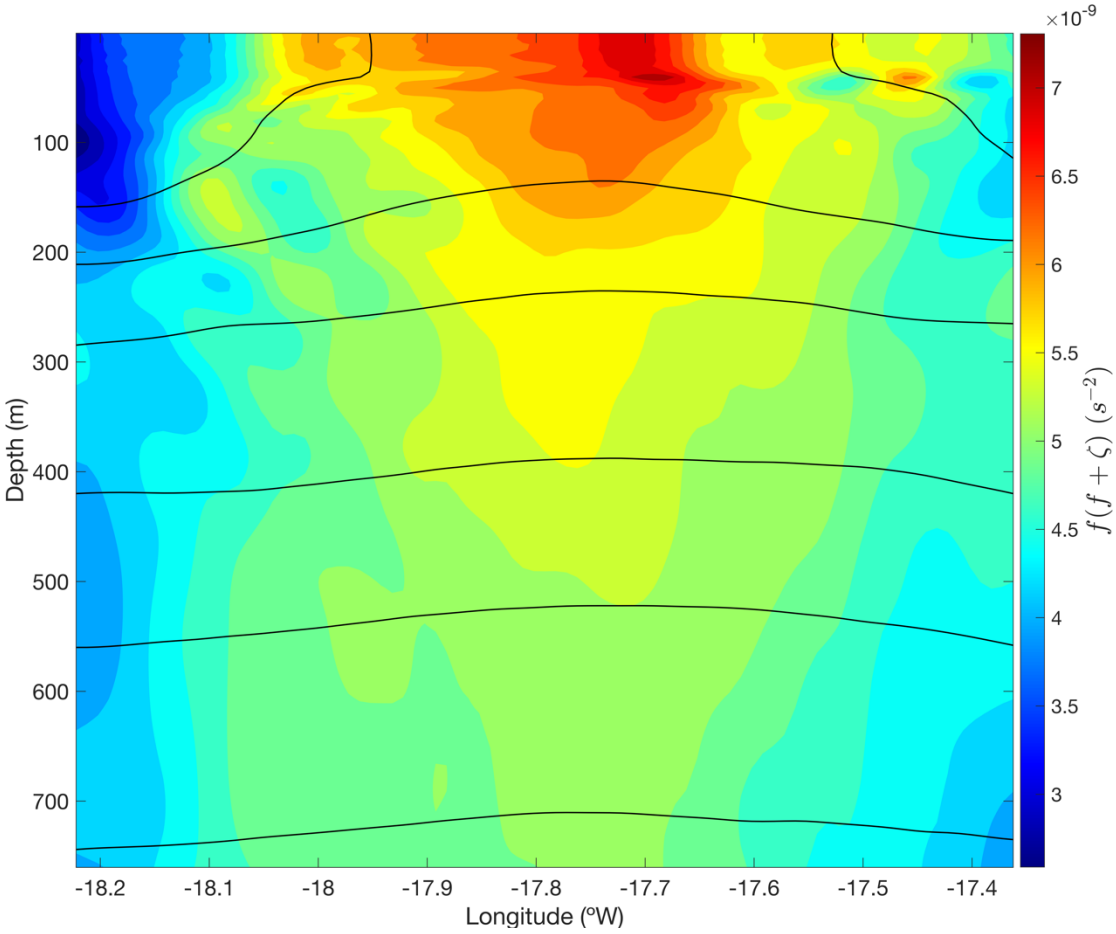

Figure 4: Total vorticity, using the IBI data, for the same water column as Figure 3. Note that the total vorticity has been multiplied by the constant value of the Coriolis parameter.

The remaining terms on the right-hand side of equation (12) represent the forcing terms of the generalized omega equation. On the one hand, the $\boldsymbol{Q}$ vector represents the deformation of the horizontal density gradient by the horizontal velocity field; thus, its divergence is related to the total deformation field, and it can be decomposed into geostrophic and ageostrophic components.

As it can be seen in Figure 5 the major contribution to the total deformation field will be due to the ageostrophic components of the horizontal velocity. The geostrophic velocity refers to the speed at which a particle would move in a fluid at equilibrium under the influence of the Coriolis force and the horizontal pressure gradient. This velocity is proportional to the distance from the center of the vortex and is higher in the outer part of the vortex. On the other hand, the agesostrophic velocity refers to any additional velocity in an eddy that is not in geostrophic equilibrium, such as acceleration towards

the center of the eddy or the influence of frictional forces. This explains why the agesostrophic velocity has a greater influence on the total deformation at shallow depths, where there is greater acceleration towards the center of the eddy and therefore greater deformation of the density field, as we see in the isopycnal in Figure 5 that runs from 150 meters to the surface.

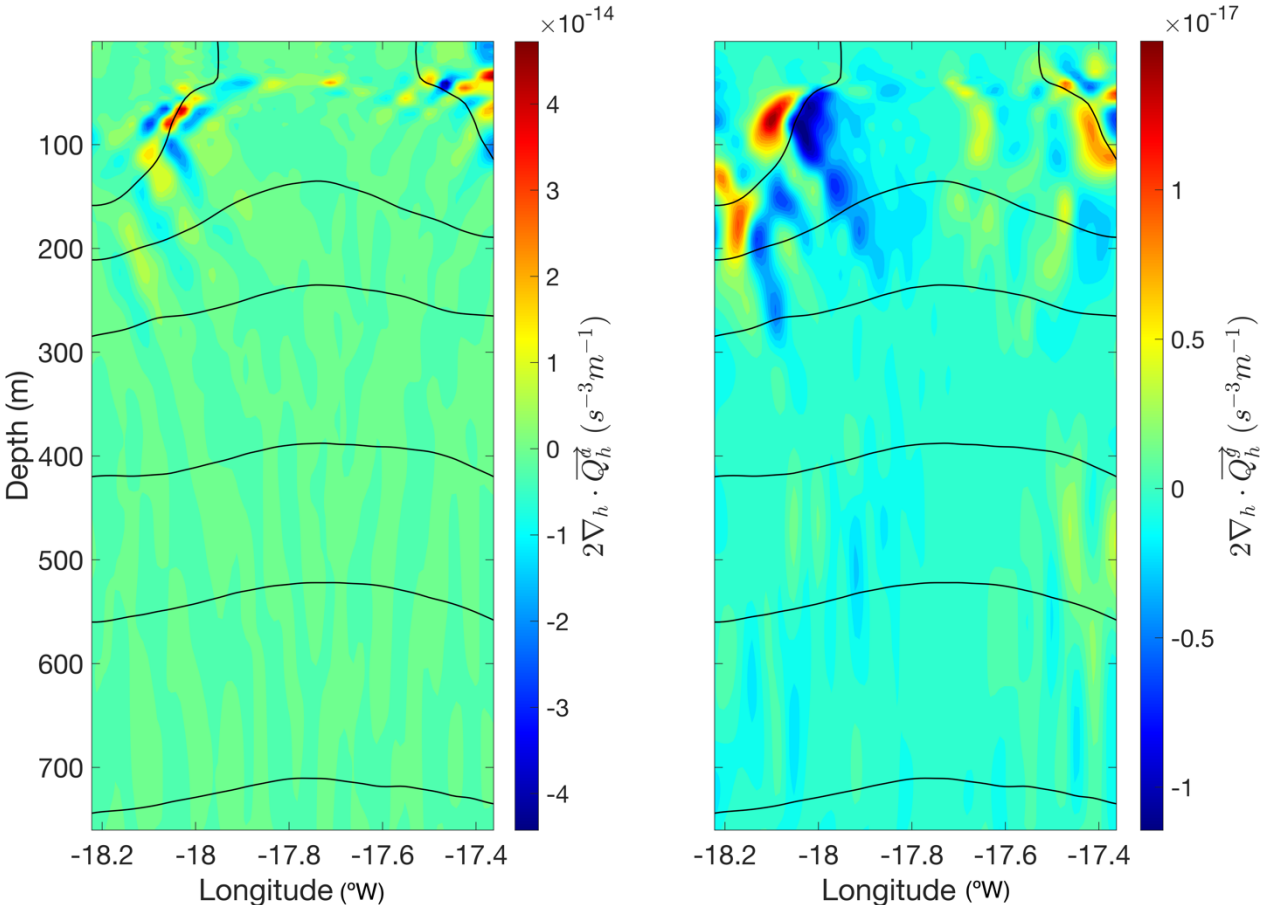

Figure 5: Total deformation field for the water column: the left figure is due to ageostrophic and the right figure to geostrophic components.

A background can be observed in Figure 5, likely associated with the errors propagated by the derivatives. This would make it difficult to obtain the vertical velocity pattern, which will be discussed in more detail in the next section.

The term $\boldsymbol{\zeta}_{ph}^{a}$ can be thought of as the anticlockwise rotation of the thermal wind imbalance as $\boldsymbol{TWI} = f(u_z^a, v_z^a)$, and hence $f\boldsymbol{\zeta}_{ph}^{a} = \boldsymbol{k} \times \boldsymbol{TWI}$ (Giordani et al. 2006). Giordani et al. (2006) also relate $f\boldsymbol{\xi}_{ph}^{a} \cdot \boldsymbol{\nabla}_h^2 \boldsymbol{u}_h$ to the stretching and reorientation of the pre-existing $\boldsymbol{\zeta}_{ph}^{a}$ by the total horizontal current field.

As it can be seen in Figure 6, the maximum of the thermal wind imbalance variation in the normal direction of the flow matches the center of the eddy and its edge.

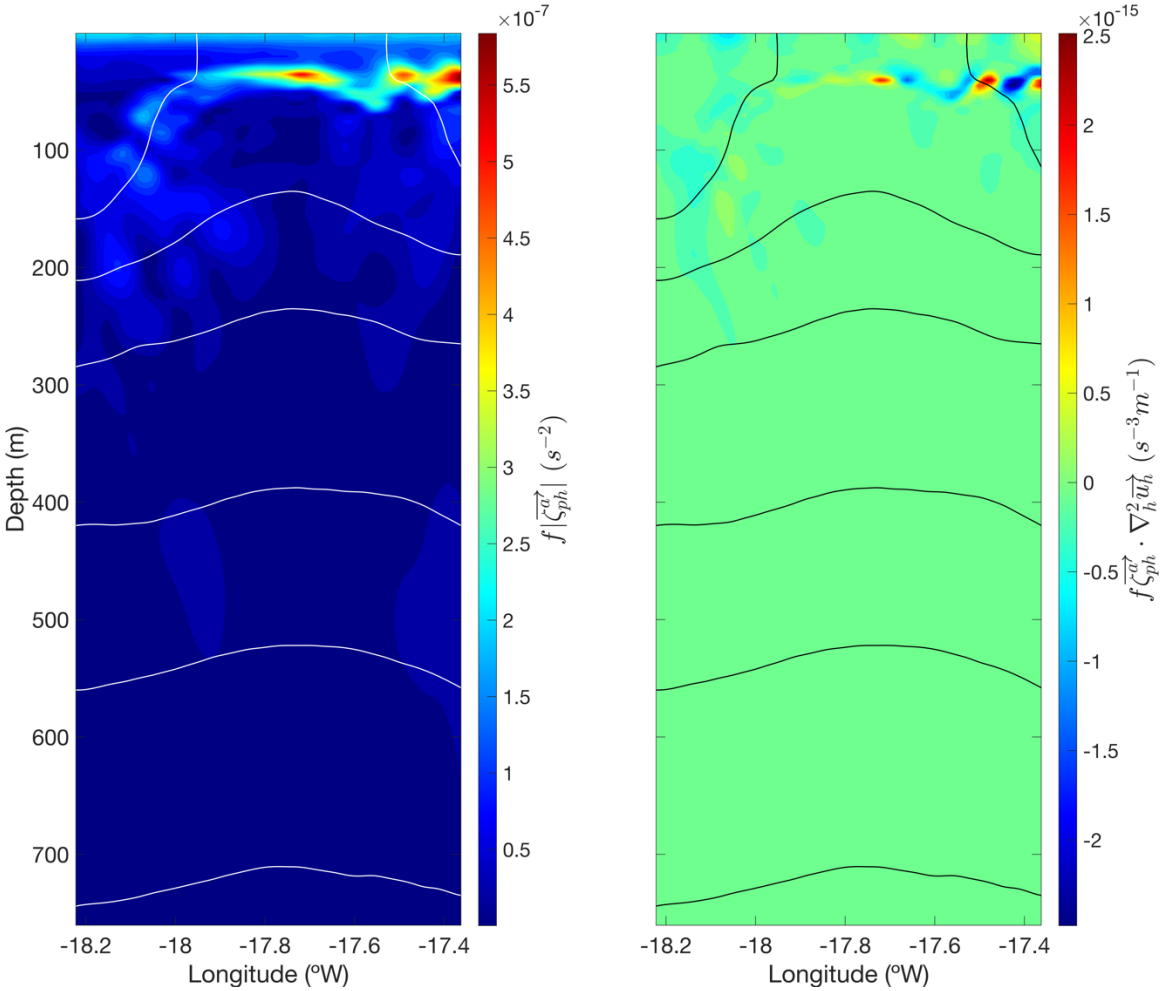

Figure 6: The anticlockwise rotation of the thermal wind imbalance on the left. The term related to the vertical shear of the horizontal ageostrophic current through $\boldsymbol{\zeta}_{ph}^{a}$ on the right, both for the same water column.

3.1.3 Background error analysis

Several parameters used in the procedure for determining the vertical velocity exhibit an error-like background structure. These parameters are obtained by calculating gradients repeatedly. The top contours in Figure 7 show this structure in the total deformation field. This pattern is also observed when the parameter is calculated usin Python with a different library, suggesting that the error is not due to the Matlab program or the EOS-80 library.

Although a small discrepancy is observed in the maximum value at a depth of approximately 50 meters between the Python and Matlab calculations in the mean profiles in Figure 7, the general shape and values are consistent. From a depth of 200 meters, the mean value oscillates around zero, indicating that the background error may be negligible.

Further testing is required to determine whether this background structure is due to signal or noise.

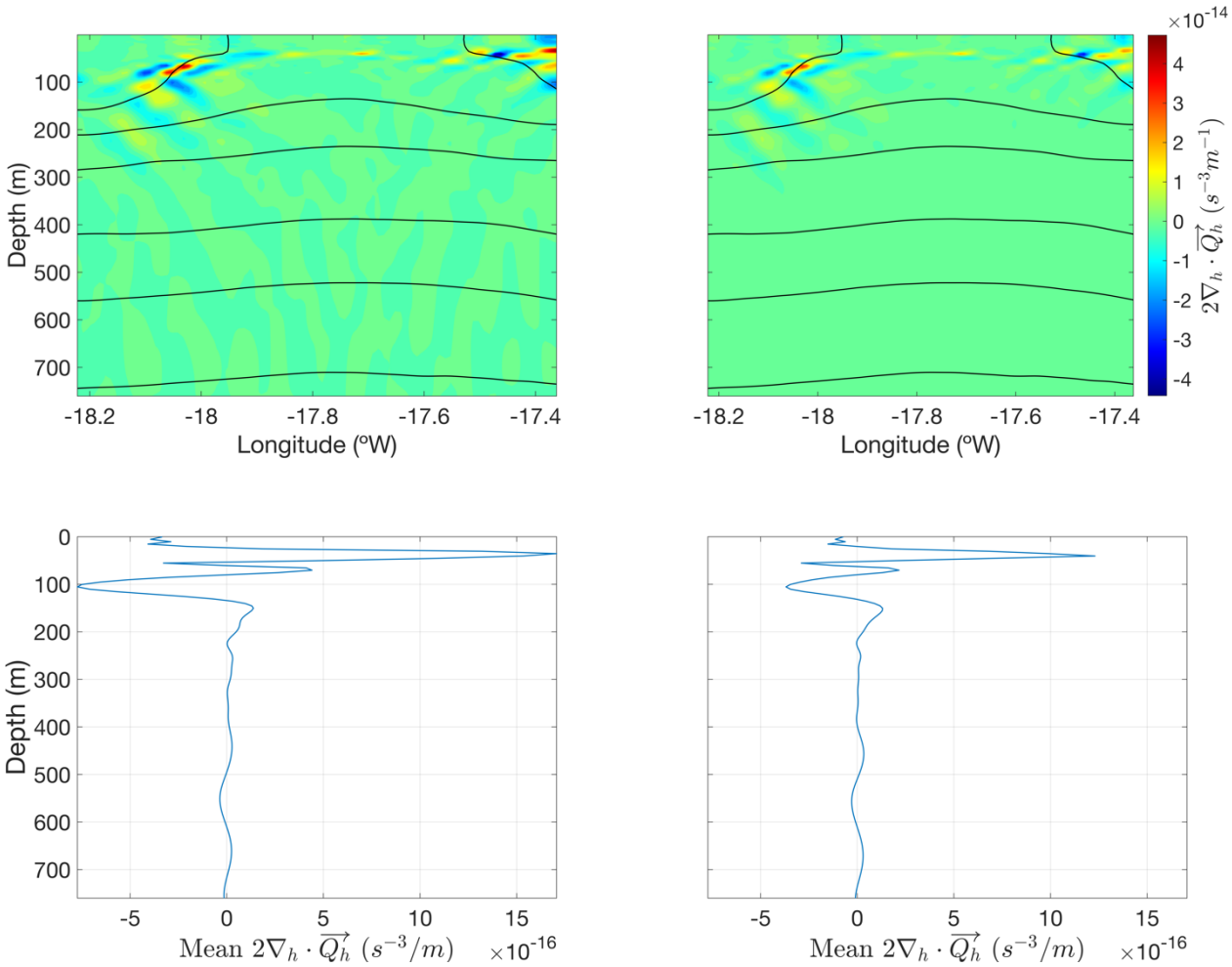

Figure 7: The contours above are the total deformation field and the plots below are the mean profiles of these fields for each depth. The graphs in the left column are made with Matlab and those on the right with Python.

3.1.4 Vertical velocity

Figure 8 displays vertical velocity ranges between [-10 and 10] m/day for depths above 300 meters. The alternating structure of positive/negative vertical velocities creates challenges in identifying a clear pattern of the vertical velocity. This structure is associated to the uppermost isopycnal and connects the eddy's core to its edge through tilted cells. The pattern appears to be isotropic, with a similar structure on both sides of the eddy.

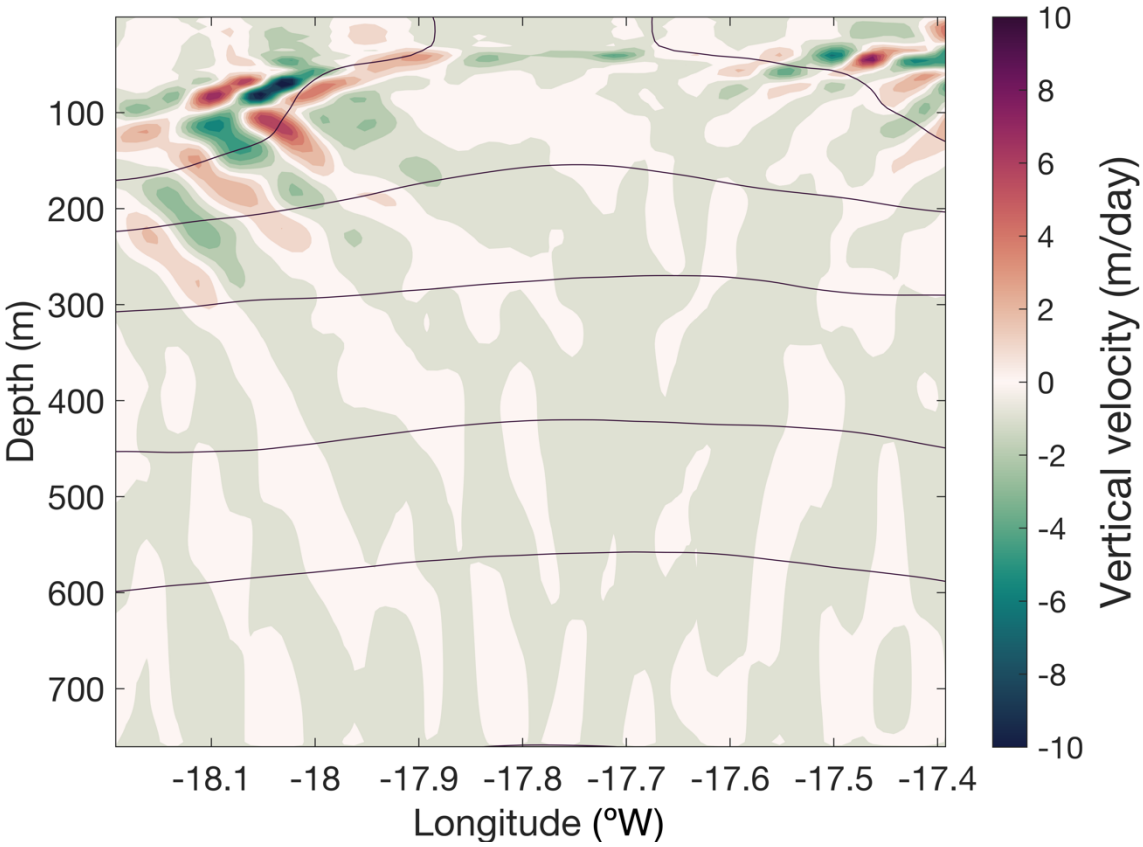

Figure 8: Vertical velocity contour for the water column, calculated from the IBI data and obtained by numerically solving the generalized omega equation.

3.2 Discussion

In discussing the data, it is worth noting that our study only sampled the eddy in situ via a CTD transect that crossed its center (Figure 1). Therefore, using the omega equation solely based on these CTD stations results in inaccurate vertical velocity calculations due to the limited in situ data. Although this approach was initially intended approach for the final degree project, a grid of CTD data was necessary to overcome this methodological limitation. To obtain a more comprehensive dataset, we utilized the IBI database.

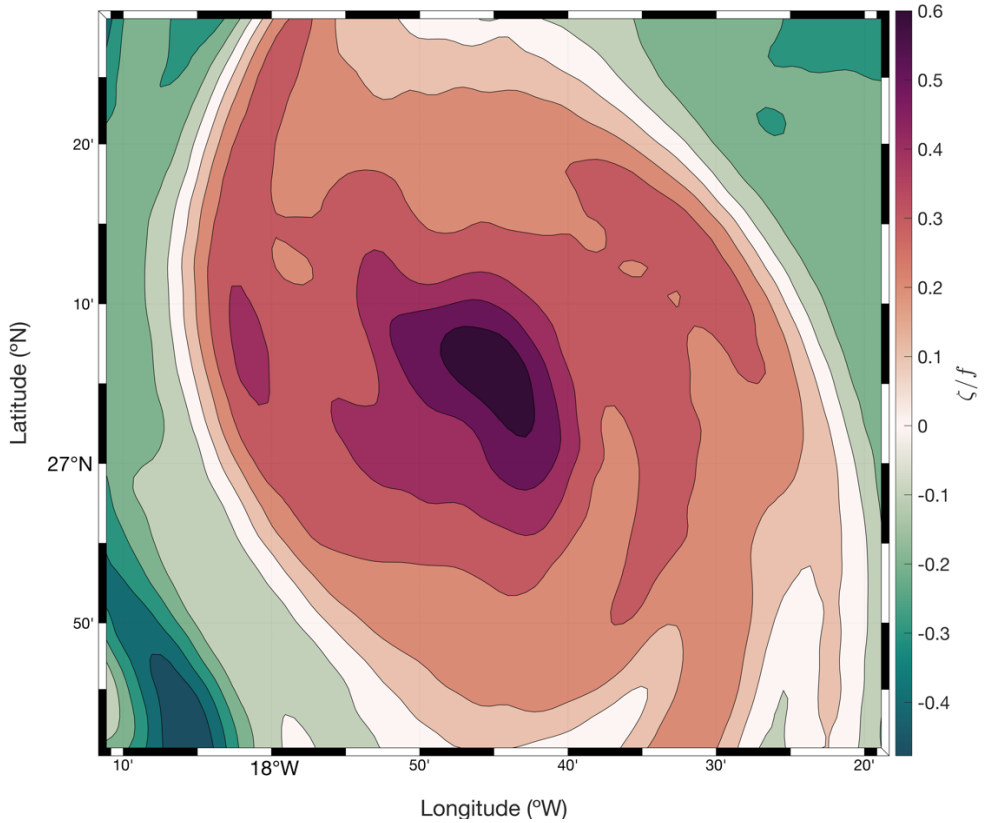

Figure 9: Rossby number for the surface of the eddy at 10 m depth.

The possibility of using synthetic in situ data was initially considered but ultimately discarded due to the absence of horizontal current velocity measurements caused by a damaged ADCP. Furthermore, the quasi-geostrophic theory could not be applied due to the Rossby number approaching 1 in areas close to the eddy's center (Figure 9). This means that fluid acceleration effects are significant, making the use of synthetic data without ADCP velocity infeasible.

Concerning the cubic interpolation applied on the IBI data and its effect on the results, it was found that, in some cases, the interpolation smoothed or varied the parameter plots, but in general, the results remained unchanged. A more detailed study of non-linear interpolations in eddies using this dataset would be required to determine the best interpolation scheme.

Regarding the results obtained, one worth highlighting is from section 3.1.1, where the geostrophic velocity of the in situ data was compared with the interpolated information in the same coordinates and depths of the IBI data. As shown in Figure 2, the result is very similar in both shape and numerical values, except for the smoother model result as compared to the in situ data. The model assimilates the input data by incorporating in situ data of temperature and salinity profiles, Sea Surface Temperature (SST), and Sea Surface Height (SSH) from satellite data, with smoothing being applied to the latter two (Sotillo et al. 2015). This result suggests that the model has adequate resolution to assimilate the horizontal hydrodynamics of an eddy, at least.

In terms of cyclonic eddy's parameters, nothing seems unusual except for the presence of a possible constant noise structure in most of the parameters where multiple derivatives are performed, particularly in all the parameters associated with the ageostrophic components of equation (15).

By isolating the iterative term of the omega equation $F(x_i, y_j, z_k)$ from equation (16), we see that for boundary conditions at $\omega|_{z=700} = 0$ and near-zero side conditions, the dominant term in this area is equation (15), resulting in negative solutions to $F(x_i, y_j, z_k)$ as seen in Figure 8. If $C(x_i, y_j, z_k)$ presents a background noise structure, these values will propagate to the solution of the omega equation in this zone, and consequently, to the rest of the solutions of the grid solutions.

Several factors may cause the noise in the ageostrophic components. The optimal interpolation for each eddy must be studied in detail, including implementing filters for certain scales, which were not considered in this case. Additionally, the IBI data have low resolution at high depths, where this noise pattern was observed, and due to the high variability in these structures, the vertical interpolation may not be helpful. As seen in Figure 10, the CTD contours have higher variability at high depths, while the IBI ones have smoother and more regular contours at these depths, with a variation in regularity at approximately 500 m, where it coincides with the increase of the vertical resolution of the IBI dataset. Due to this smoothness and regularity, the multiple derivatives performed to obtain most parameters may propagate an error causing the background pattern.

Figure 11 shows that there is a noticeable difference between the temperature and salinity data obtained from the IBI dataset and the CTD stations. At a depth of 100 m, the difference is of 1.5°C in temperature and 0.3 in salinity. Additionally, a bulb-shaped isopycnal is observed between the 50 and 100 m depths of the IBI data, which is not seen with the CTD stations. Independent studies have been conducted to evaluate the reliability of these models, using various instruments such as Argo floats, tide gauges, buoys, and high-frequency radars. These studies estimate a maximum error of 1°C and 0.2 in salinity (Lellouche et al. 2013). The relatively small discrepancy between the error estimate and the observed difference may be due to the fact that the CTD data were collected between 8 am to 20 pm, whereas the IBI dataset is averaged over entire day. This temporal averaging may account for the small variation observed.

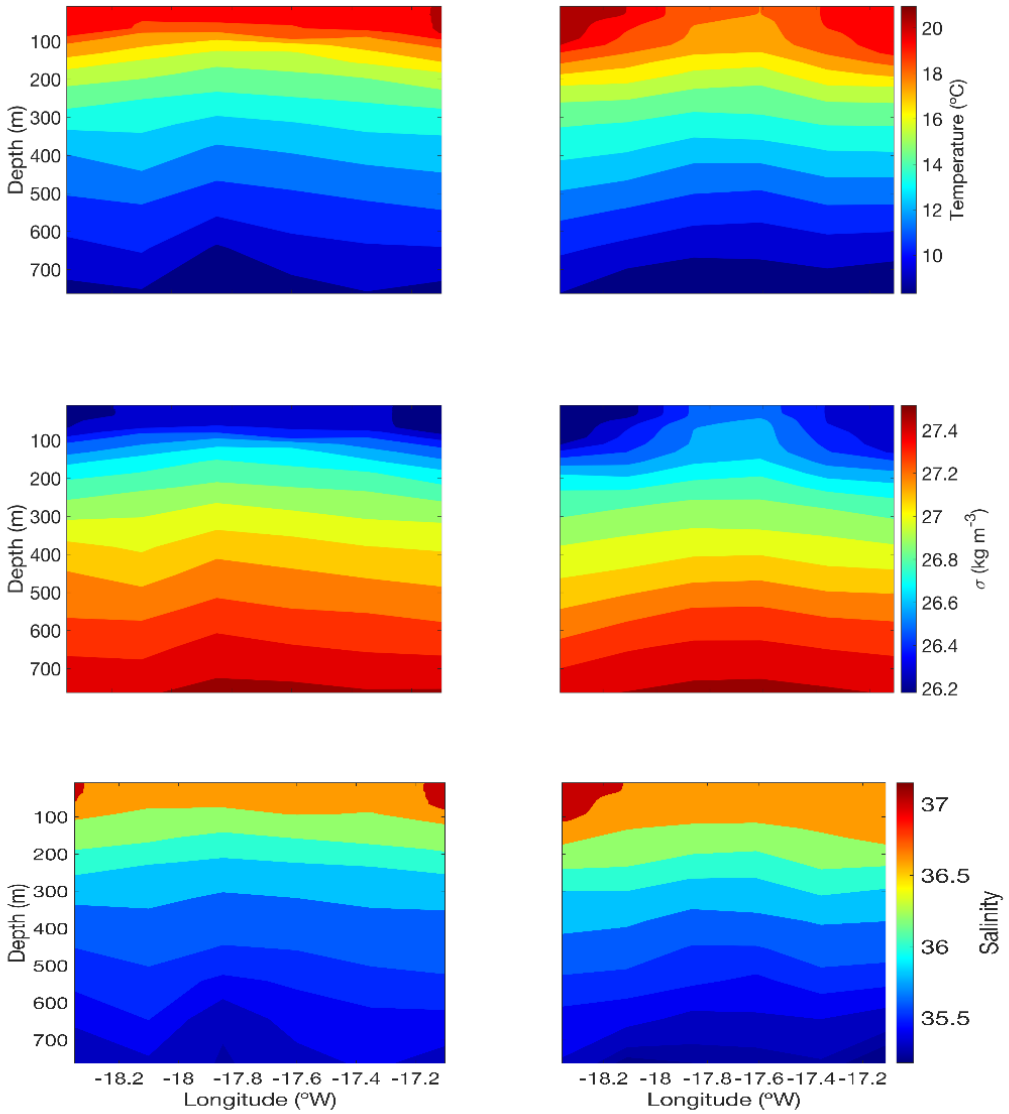

Figure 10: The left column presents temperature, density anomaly and salinity data for the water column from the CTD stations and the right column does the same from the pseudo-stations with the IBI dataset.

A recent report by the Mediterranean Institute for Advanced Studies (IMEDEA) - CSIC-UIB (Hermilly and Ruiz, 2021) supports the hypothesis that the smoothness of the IBI model can impact the results of vertical velocity obtained through the omega equation. The report describes the measurement of vertical velocity in a gyre of strong activity in the Alboran Sea during the Calypso 2018 experiment, using uCTD and surface drifters. Results obtained using QG omega equation with the IBI model data were compared with the in situ measurements, which were consistent, while the IBI results, in the same way of our results, underestimated the value of the vertical velocity.

The report concludes that the displacement of features and the smoothness of the model output resulted in errors in the location, intensity, and sizes of the vertical velocities compared to both uCTD and drifter results. This underestimation occurred in an area of high activity where the vertical velocities were significantly higher compared to those of a mesoscale eddy that had been forming for 5 months, similar to the present study. The low intensity of the vertical velocity and the difficulty in obtaining it with IBI may result in background errors, making it difficult to obtain a clear pattern. These results support the notion that while the IBI model has sufficient resolution to resolve a mesoscale eddy, it lacks the necessary tools to obtain an accurately measure vertical velocity.

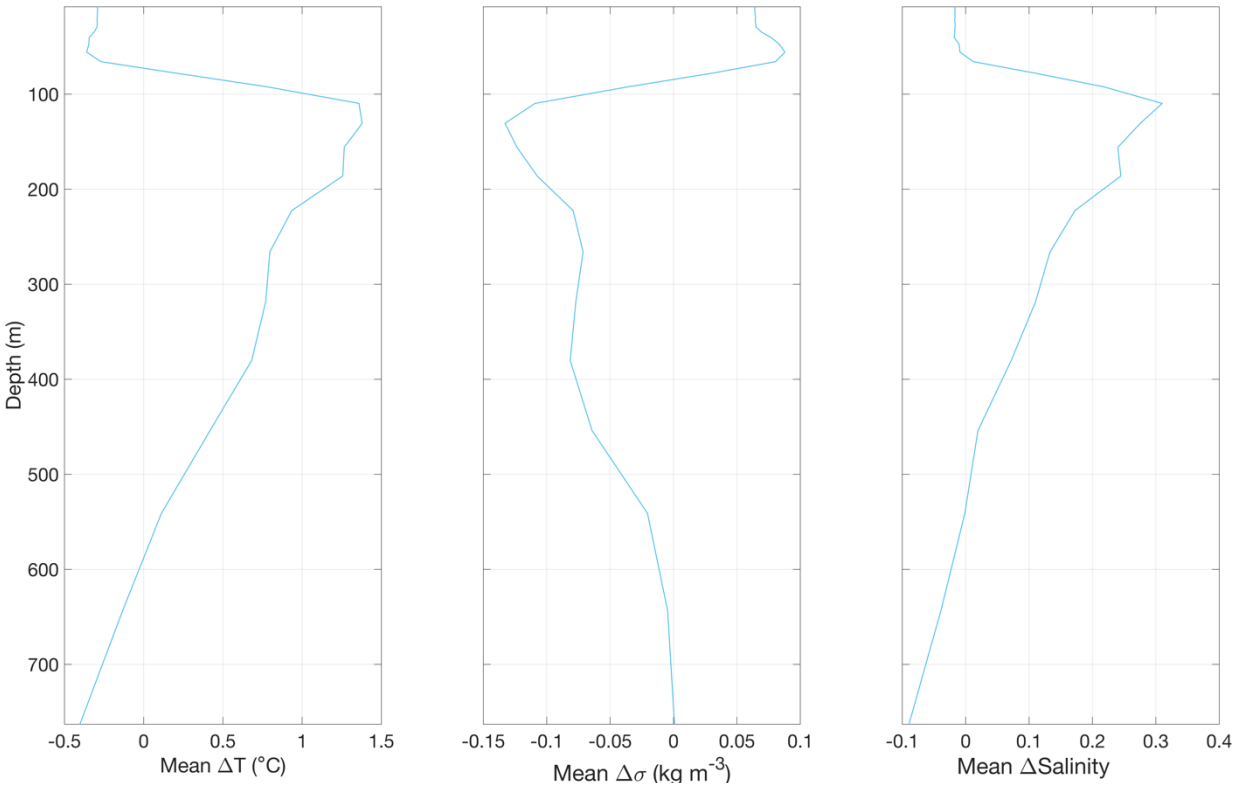

Figure 11: Profiles of the mean value of the difference between IBI model and CTD station data for temperature, density and salinity, for the water column.

Chapter 4

Conclusion and future work

Resumen:

Este capítulo expone las conclusiones previamente justificadas y pone de manifiesto la originalidad del trabajo. También se proponen futuras líneas de investigación en relación con el estudio de las velocidades verticales en estructuras mesoescalares.

4.1 Conclusion

This final undergraduate project aims to introduce physical oceanography from a perspective and the quasigeostrophic theory of dynamic meteorology. The work is innovative in its approach of solving the vertical velocity of an ocean eddy using a partial differential equation with model data and comparing it with information obtained from an oceanographic cruise. It provides an introduction to the experimental tools commonly used in physical oceanography and emphasizes the importance of correctly measuring mesoscale structures in the ocean.

The findings of this study highlighted the limitations of the Copernicus IBI model in accurately estimating the vertical velocity of not just highly active mesoscale structures in the Alboran Sea, but also for medium to low-active mesoscale structures commonly observed in the Canary Island Archipelago. The work highlights the model's low vertical resolution, its smoothness, and the errors that propagate through multiple calculations of partial derivatives. The study also verifies the model output data, such as temperature and salinity, with in situ measurements and confirms that the values are within the expected error range.

4.2 Future work

This work has shown that obtaining an accurate value of the vertical velocity presents major challenges both experimentally and from a modeling perspective. The weak intensity of the vertical field in comparison with the horizontal currents makes it difficult to measure accurately. Mesoscale structures are interesting places to measure the vertical velocity, where the activity is greater and the vertical velocity is higher, but these structures are very sensitive to observational errors, the distribution of stations, and the synopticity of the sampling. Morewover, the non-linearity of these structures requires

the use of Optimal Statistical Interpolation (OI) formulation, and scale selection or spatial filtering must be applied to suppress small scales that cannot be resolved by the station distribution (Gomis and Pedder 2005).

As a result, future work is proposed, which includes optimal sampling of an eddy and other mesoscale structures near the Canary coast, with a good spatial resolution and with the possibility of implementing LADCPs, which allows the calculation of vertical velocity profiles and would serve as an additional measure to contrast the results. It is also important to search and improve other models that allow solving the vertical velocity by means of an omega equation, or, if necessary, creating a new model that uses altimetry data and Argo profilers. The Spanish Institute of Oceanography is very involved in this project. Additionally, the data available from the BIOCAN98 oceanographic cruise can be used for further study, as two eddies were sampled with a regular grid, and the results were used for the analysis of the mixing processes in the eddy (Arcos-Pulido 2013) without studying the advection processes, which are the subject of this final degree work.

Bibliography

Allen, J. T., and D. A. Smeed, 1996: Potential Vorticity and Vertical Velocity at the Iceland-Færœs Front. *J Phys Oceanogr*, **26**, 2611–2634, https://doi.org/10.1175/1520-0485(1996)026.

Arcos-Pulido, M., 2013: Difusividad turbulenta vertical y suministro de nutrientes en la Cuenca de Canarias. .

Barceló-Llull, B., E. Mason, A. Capet, and A. Pascual, 2016: Impact of vertical and horizontal advection on nutrient distribution in the southeast Pacific. *Ocean Science*, **12**, 1003–1011, https://doi.org/10.5194/OS-12-1003-2016.

Benítez-Barrios, V. M., J. L. Pelegrí, A. Hernández-Guerra, K. M. M. Lwiza, D. Gomis, P. Vélez-Belchí, and S. Hernández-León, 2011a: Three-dimensional circulation in the NW Africa coastal transition zone. *Prog Oceanogr*, **91**, 516–533, https://doi.org/10.1016/J.POCEAN.2011.07.022.

——, ——, ——, ——, ——, ——, and ——, 2011b: Three-dimensional circulation in the NW Africa coastal transition zone. *Prog Oceanogr*, **91**, 516–533, https://doi.org/10.1016/J.POCEAN.2011.07.022.

Brian J. Hoskins, and Ion Draghici, 1977: The Forcing of Ageostrophic Motion According to the Semi-Geostrophic Equations and in an Isentropic Coordinate Model in: Journal of the Atmospheric Sciences Volume 34 Issue 12 (1977). *American Meteorological Society*, 1859–1867. https://journals.ametsoc.org/view/journals/atsc/34/12/1520-0469_1977_034_1859_tfoama_2_0_co_2.xml?tab_body=pdf (Accessed December 29, 2022).

Chelton, D. B., and S. P. Xie, 2010: Coupled ocean-atmosphere interaction at oceanic mesoscales. *Oceanography*, **23**, 54–69, https://doi.org/10.5670/oceanog.2010.05.

Estrada-Allis, S. N., B. Barceló-Llull, E. Pallàs-Sanz, A. Rodríguez-Santana, J. M. A. C. Souza, E. Mason, J. C. Mcwilliams, and P. Sangrà, 2019: Vertical velocity dynamics and mixing in an anticyclone near the Canary Islands. *J Phys Oceanogr*, **49**, 431–451, https://doi.org/10.1175/JPO-D-17-0156.1.

Gaube, P., D. B. Chelton, R. M. Samelson, M. G. Schlax, and L. W. O'Neill, 2015: Satellite Observations of Mesoscale Eddy-Induced Ekman Pumping. *J Phys Oceanogr*, **45**, 104–132, https://doi.org/10.1175/JPO-D-14-0032.1.

Giordani, H., L. Prieur, and G. Caniaux, 2006: Advanced insights into sources of vertical velocity in the ocean. *Ocean Dyn*, **56**, 513–524, https://doi.org/10.1007/S10236-005-0050-1/FIGURES/5.

Gomis, D., and M. A. Pedder, 2005: Errors in dynamical fields inferred from oceanographic cruise data: Part I. The impact of observation errors and the sampling distribution. *Journal of Marine Systems*, **56**, 317–333, https://doi.org/10.1016/J.JMARSYS.2005.02.002.

Gregory, J. M., 2000: Vertical heat transports in the ocean and their effect on time-dependent climate change. *Clim Dyn*, **16**, 501–515, https://doi.org/10.1007/S003820000059/METRICS.

Hansen, D. v, C. A. Paul, D. v Hansen, and C. A. Paul, 1987: OCEANOLOGICA ACTA, 1987, N° SP 0 Vertical motion Upwelling Vertical motion Equatorial currents

Drifting buoys Pacific Ocean in the Eastern equatorial Pacific inferred from drifting buoys Upwelling Mouvement vertical Courants équatoriaux Bouées dérivantes Océan Pacifique ABSTRACT RÉSUMÉ Mouvement vertical dans l'est du Pacifique à partir de bouées dérivantes "l '. *Oceanol. Acta*, 27–32.

Harcourt, R. R., E. L. Steffen, R. W. Garwood, and E. A. D'asaro, 2002: *Fully Lagrangian Floats in Labrador Sea Deep Convection: Comparison of Numerical and Experimental Results*.

Hermilly, T., and S. Ruiz, 2021: *Report on the representation of vertical velocities in the Iberian Biscay Irish Ocean Analysis and Forecasting system using multi-platform observations*. CSIC-UIB - Instituto Mediterráneo de Estudios Avanzados (IMEDEA), https://digital.csic.es/handle/10261/268500 (Accessed March 1, 2023).

Hoskins, B. J., I. Draghici, and H. C. Davies, 1978: A new look at the ω-equation. *Quarterly Journal of the Royal Meteorological Society*, **104**, 31–38, https://doi.org/10.1002/QJ.49710443903.

Houtman, H., F. W. Jones, and C. J. Kost, 1994: Laplace and Poisson equation solution by relax3d. *Citation: Computers in Physics*, **8**, 469, https://doi.org/10.1063/1.168506.

Joaquín Tintoré, Damià Gomis, Sergio Alonso, and Gregorio Parrilla, 1991: Mesoscale Dynamics and Vertical Motion in the Alborán Sea in: Journal of Physical Oceanography Volume 21 Issue 6 (1991). *American Meteorological Society*, 811–823. https://journals.ametsoc.org/view/journals/phoc/21/6/1520-0485_1991_021_0811_mdavmi_2_0_co_2.xml?tab_body=pdf (Accessed December 29, 2022).

Klein, P., and G. Lapeyre, 2009: The Oceanic Vertical Pump Induced by Mesoscale and Submesoscale Turbulence. *https://doi.org/10.1146/annurev.marine.010908.163704*, **1**, 351–375, https://doi.org/10.1146/ANNUREV.MARINE.010908.163704.

Klocker, A., and R. Abernathey, 2014: Global Patterns of Mesoscale Eddy Properties and Diffusivities. *J Phys Oceanogr*, **44**, 1030–1046, https://doi.org/10.1175/JPO-D-13-0159.1.

Kooi, M., E. H. van Nes, M. Scheffer, and A. A. Koelmans, 2017: Ups and Downs in the Ocean: Effects of Biofouling on Vertical Transport of Microplastics. *Environ Sci Technol*, **51**, 7963–7971, https://doi.org/10.1021/ACS.EST.6B04702/ASSET/IMAGES/LARGE/ES-2016-047026_0003.JPEG.

Leach, H., 1987: The diagnosis of synoptic-scale vertical motion in the seasonal thermocline. *Deep Sea Research Part A. Oceanographic Research Papers*, **34**, 2005–2017, https://doi.org/10.1016/0198-0149(87)90095-1.

Lellouche, J. M., and Coauthors, 2013: Evaluation of global monitoring and forecasting systems at Mercator Océan. *Ocean Science*, **9**, 57–81, https://doi.org/10.5194/OS-9-57-2013.

Mahadevan, A., 2016: The Impact of Submesoscale Physics on Primary Productivity of Plankton. *https://doi.org/10.1146/annurev-marine-010814-015912*, **8**, 161–184, https://doi.org/10.1146/ANNUREV-MARINE-010814-015912.

——, and A. Tandon, 2006: An analysis of mechanisms for submesoscale vertical motion at ocean fronts. *Ocean Model (Oxf)*, **14**, 241–256, https://doi.org/10.1016/J.OCEMOD.2006.05.006.

——, L. N. Thomas, and A. Tandon, 2008: Comment on "eddy/wind interactions stimulate extraordinary mid-ocean plankton blooms." *Science (1979)*, **320**, https://doi.org/10.1126/SCIENCE.1152111/SUPPL_FILE/MAHADEVAN_SOM.PDF.

Martin, A. P., and K. J. Richards, 2001: Mechanisms for vertical nutrient transport within a North Atlantic mesoscale eddy. *Deep Sea Res 2 Top Stud Oceanogr*, **48**, 757–773, https://doi.org/10.1016/S0967-0645(00)00096-5.

McGillicuddy, D. J., 2016: Mechanisms of Physical-Biological-Biogeochemical Interaction at the Oceanic Mesoscale. *Ann Rev Mar Sci*, **8**, 125–159, https://doi.org/10.1146/annurev-marine-010814-015606.

McWilliams, J. C., 2008: The Nature and Consequences of Oceanic Eddies. *Geophysical Monograph Series*, **177**, 5–15, https://doi.org/10.1029/177GM03.

Nagai, T., A. Tandon, and D. L. Rudnick, 2006: Two-dimensional ageostrophic secondary circulation at ocean fronts due to vertical mixing and large-scale deformation. *J Geophys Res Oceans*, **111**, 9038, https://doi.org/10.1029/2005JC002964.

Nardelli, B. B., 2013: Vortex waves and vertical motion in a mesoscale cyclonic eddy. *J Geophys Res Oceans*, **118**, 5609–5624, https://doi.org/10.1002/JGRC.20345.

Ning, X., F. Chai, H. Xue, Y. Cai, C. Liu, and J. Shi, 2004: Physical-biological oceanographic coupling influencing phytoplankton and primary production in the South China Sea. *J Geophys Res Oceans*, **109**, 10005, https://doi.org/10.1029/2004JC002365.

P. Morgan, P., 1994: *A Library of MATLAB Computational Routines for the Properties of Sea Water*. CSIRO Marine Laboratories, Ed.

Pallàs-Sanz, E., T. M. S. Johnston, and D. L. Rudnick, 2010a: Frontal dynamics in a California Current System shallow front: 1. Frontal processes and tracer structure. *J Geophys Res Oceans*, **115**, https://doi.org/10.1029/2009JC006032.

——, ——, and ——, 2010b: Frontal dynamics in a California Current System shallow front: 2. Mesoscale vertical velocity. *J Geophys Res Oceans*, **115**, https://doi.org/10.1029/2010JC006474.

Pascual, A., Y. Faugère, G. Larnicol, and P. Y. le Traon, 2006: Improved description of the ocean mesoscale variability by combining four satellite altimeters. *Geophys Res Lett*, **33**, https://doi.org/10.1029/2005GL024633.

——, S. Ruiz, B. Buongiorno Nardelli, S. Guinehut, D. Iudicone, and J. Tintoré, 2015: Net primary production in the Gulf Stream sustained by quasi-geostrophic vertical exchanges. *Geophys Res Lett*, **42**, 441–449, https://doi.org/10.1002/2014GL062569.

Pedder, M. A., and A. J. Thorpe, 1999: The semi-geostrophic diagnosis of vertical motion. I: Formulation and coordinate transformations. *Quarterly Journal of the Royal Meteorological Society*, **125**, 1231–1256, https://doi.org/10.1002/QJ.1999.49712555607.

Pierre, I., S. Laplace, G. Madec, and P. Delecluse, 2008: Notes du Pôle de Modélisation OPA 8.1 Ocean General Circulation Model Reference Manual.

Pinot, J. M., J. Tintoré, and D. P. Wang, 1996: A study of the omega equation for diagnosing vertical motions at ocean fronts. *J Mar Res*, **54**, 239–259, https://doi.org/10.1357/0022240963213358.

Pollard, R. T., and L. A. Regier, 1992: Vorticity and Vertical Circulation at an Ocean Front. *J Phys Oceanogr*, **22**, 609–625,

https://doi.org/https://doi.org/10.1175/1520-0485(1992)022%3C0609:VAVCAA%3E2.0.CO;2.

S. S. Lindstrom, and D. P. Watts, 1994: Vertical Motion in the Gulf Stream Near 68°W in: Journal of Physical Oceanography Volume 24 Issue 11 (1994). https://journals.ametsoc.org/view/journals/phoc/24/11/1520-0485_1994_024_2321_vmitgs_2_0_co_2.xml?tab_body=pdf (Accessed December 28, 2022).

Samuelsen, A., S. S. Hjøllo, J. A. Johannessen, and R. Patel, 2012: Particle aggregation at the edges of anticyclonic eddies and implications for distribution of biomass. *Ocean Science*, **8**, 389–400, https://doi.org/10.5194/OS-8-389-2012.

Sotillo, M. G., and Coauthors, 2015: The MyOcean IBI Ocean Forecast and Reanalysis Systems: operational products and roadmap to the future Copernicus Service. *https://doi.org/10.1080/1755876X.2015.1014663*, **8**, 63–79, https://doi.org/10.1080/1755876X.2015.1014663.

Stern, M. E., 1965: Interaction of a uniform wind stress with a geostrophic vortex. *Deep Sea Research and Oceanographic Abstracts*, **12**, 355–367, https://doi.org/10.1016/0011-7471(65)90007-0.

Trenberth, K. E., 1977: *On the interpretation of the diagnostic quasi-geostrophic omega equation*. 131–137 pp.

Viúdez, Á., and D. G. Dritschel, 2004: Potential Vorticity and the Quasigeostrophic and Semigeostrophic MesoscaleVertical Velocity. *J Phys Oceanogr*, 865–887. https://journals.ametsoc.org/view/journals/phoc/34/4/1520-0485_2004_034_0865_pvatqa_2.0.co_2.xml?tab_body=fulltext-display (Accessed December 30, 2022).

——, J. Tintoré, and R. L. Haney, 1996: About the Nature of the Generalized Omega Equation in: Journal of the Atmospheric Sciences Volume 53 Issue 5 (1996). *American Meteorological Society*, 787–795. https://journals.ametsoc.org/view/journals/atsc/53/5/1520-0469_1996_053_0787_atnotg_2_0_co_2.xml (Accessed December 28, 2022).

Zhang, J., 1998: Fast and High Accuracy Multigrid Solution of the Three Dimensional Poisson Equation. *J Comput Phys*, **143**, 449–461, https://doi.org/10.1006/JCPH.1998.5982.